

This is a repository copy of *The effect of varying jaw-elevator muscle forces on a finite element model of a human cranium.*

White Rose Research Online URL for this paper:  
<https://eprints.whiterose.ac.uk/99305/>

Version: Accepted Version

---

**Article:**

Toro-Ibacache, Viviana and O'Higgins, Paul [orcid.org/0000-0002-9797-0809](https://orcid.org/0000-0002-9797-0809) (2016) The effect of varying jaw-elevator muscle forces on a finite element model of a human cranium. *Anatomical Record: Advances in Integrative Anatomy and Evolutionary Biology*. ISSN 1932-8494

<https://doi.org/10.1002/ar.23358>

---

**Reuse**

Items deposited in White Rose Research Online are protected by copyright, with all rights reserved unless indicated otherwise. They may be downloaded and/or printed for private study, or other acts as permitted by national copyright laws. The publisher or other rights holders may allow further reproduction and re-use of the full text version. This is indicated by the licence information on the White Rose Research Online record for the item.

**Takedown**

If you consider content in White Rose Research Online to be in breach of UK law, please notify us by emailing [eprints@whiterose.ac.uk](mailto:eprints@whiterose.ac.uk) including the URL of the record and the reason for the withdrawal request.

1 The effect of varying jaw-elevator muscle forces on a finite element model of a human  
2 cranium

3

4 Viviana Toro-Ibacache<sup>1,2</sup>, Paul O'Higgins<sup>1</sup>

5

6 <sup>1</sup> Centre for Anatomical and Human Sciences

7 Department of Archaeology and Hull York Medical School, University of York

8 Heslington

9 York YO10 5DD

10 United Kingdom

11

12 <sup>2</sup> Facultad de Odontología Universidad de Chile

13 Sergio Livingstone Pohlhammer 943

14 Independencia, Región Metropolitana

15 Chile

16

17

18 Address for Correspondence:

19 Viviana Toro-Ibacache

20 Facultad de Odontología Universidad de Chile

21 Sergio Livingstone Pohlhammer 943

22 Independencia, Región Metropolitana

23 Chile

24 Email: mtoroibacache@odontologia.uchile.cl

25 Summary

26 Finite element analyses simulating masticatory system loading are increasingly undertaken in  
27 primates, hominin fossils and modern humans. Simplifications of models and loadcases are  
28 often required given the limits of data and technology. One such area of uncertainty concerns  
29 the forces applied to cranial models and their sensitivity to variations in these forces. We  
30 assessed the effect of varying force magnitudes among jaw-elevator muscles applied to a finite  
31 element model of a human cranium. The model was loaded to simulate incisor and molar bites  
32 using different combinations of muscle forces. Symmetric, asymmetric, homogeneous and  
33 heterogeneous muscle activations were simulated by scaling maximal forces. The effects were  
34 compared with respect to strain distribution (i.e. modes of deformation) and magnitudes; bite  
35 forces and temporomandibular joint (TMJ) reaction forces. Predicted modes of deformation,  
36 strain magnitudes and bite forces were directly proportional to total applied muscle force and  
37 relatively insensitive to the degree of heterogeneity of muscle activation. However, TMJ  
38 reaction forces and mandibular fossa strains decrease and increase on the balancing and  
39 working sides according to the degree of asymmetry of loading. These results indicate that  
40 when modes, rather than magnitudes, of facial deformation are of interest, errors in applied  
41 muscle forces have limited effects. However the degree of asymmetric loading does impact on  
42 TMJ reaction forces and mandibular fossa strains. These findings are of particular interest in  
43 relation to studies of skeletal and fossil material, where muscle data are not available and  
44 estimation of muscle forces from skeletal proxies is prone to error.

45 Keywords: finite element analysis; human cranium; masticatory muscle activity; sensitivity  
46 analysis.

47 Introduction

48 Finite element analyses (FEAs) simulating masticatory system loading in crania of primates  
49 hominin fossils and modern humans are increasingly common. However data on muscle  
50 forces, required to accurately load a model to simulate a particular function are often lacking.  
51 This means that approximations and simplifications are required and the sensitivity of finite  
52 element models to these needs to be understood. Muscle force is a parameter that is of  
53 relevance in any mechanical analysis of the masticatory system. It is generally agreed that, in  
54 simple terms, the human jaw functions as a lever (Hylander, 1975; Koolstra et al., 1988;  
55 Spencer, 1998) with the temporomandibular joint (TMJ) acting as a fulcrum, the bite point as  
56 the resistance and the muscle force as the load. The magnitude of the resulting bite force is  
57 dependent on skeletal anatomy, the locations of muscle attachment sites and so, lever arm  
58 lengths as well as muscle force magnitudes. FEA has been increasingly used to predict the  
59 mechanical response of the skull to both muscle and bite forces in terms of deformation,  
60 strains and stress. These parameters are then commonly investigated in relation to  
61 evolutionary (Strait et al., 2009; Wroe et al., 2010; Smith et al., 2015b), developmental (Kupczik  
62 et al., 2009) and physiological or pathological processes and adaptations (Tanne et al., 1988;  
63 Gross et al., 2001; Koolstra and Tanaka, 2009; Ross et al., 2011; Toro-Ibacache et al., 2015b).

64 Since reliable FEA simulation depends on accurate geometry and boundary conditions  
65 (Richmond et al., 2005; Rayfield, 2007; Kupczik, 2008), anatomically and functionally accurate  
66 models should work better than simplified models. However, current methods for FE model  
67 construction cannot fully reproduce the details of skull morphology, material properties and  
68 functional loadings, particularly when these data are not available as is the situation when  
69 dealing with archaeological or fossil material. These cases pose a particular dilemma in  
70 estimating muscle forces, which raises the question of the effects of inaccurate muscle force  
71 estimation on FE model performance. Many sensitivity analyses have been carried out in  
72 relation to FEA of vertebrate crania or mandibles. These have mainly focused in the effects of  
73 omitting anatomical structures such as sutures, sinuses, the periodontal ligament, or on the  
74 effects of varying the mechanical properties of bone (Strait et al., 2005; Kupczik et al., 2007;  
75 Gröning et al., 2011; Wood et al., 2011; Bright, 2012; Fitton et al., 2015). Only two articles  
76 have assessed the effects of varying muscle parameters on the strains/stresses of FE models of  
77 non-human primate crania (Ross et al., 2005; Fitton et al., 2012). In both cases, the authors  
78 concluded that although the varying of muscle parameters impacts performance, the

79 importance of the effects should be weighed against the aims of the study. Here we aim to  
80 systematically explore the impact of errors in applied muscle forces in an FE model of a  
81 modern human cranium to better understand the consequences in hominins.

82 The maximum contractile force of a muscle can be estimated using anatomical and chemical  
83 dissection methods to measure muscle mass and fibre length and so, to estimate muscle  
84 physiological cross-sectional area (van Eijden et al., 1997; Antón, 1999) which is directly  
85 proportional to the maximum force that can be generated. This method is impractical for  
86 ethical reasons in living humans, and impossible in archaeological and fossil material. In living  
87 humans, the cross-sectional areas (CSA) of jaw-elevator muscles obtained from medical images  
88 have been proposed as a reasonable estimator of the potential maximum force of pennate  
89 muscles (Weijs and Hillen, 1985, 1986; Koolstra et al., 1988; van Spronsen et al., 1991). When  
90 the muscles are absent, like in fossil or museum material, bony marks are used to estimate CSA  
91 (Demes and Creel, 1988; Antón, 1990; O'Connor et al., 2005; Wroe et al., 2010). However, we  
92 showed in a previous study that the CSA estimation based on bone markings is not accurate in  
93 humans, leading to an overestimation of force magnitudes and, in the case of the masseter,  
94 values that do not correlate with the measured ones (Toro-Ibacache et al., 2015a).

95 Estimating the magnitude of force actually produced by a muscle during a certain task can also  
96 pose a challenge. The electromyographic (EMG) activity of a muscle while exerting maximum  
97 and sub-maximum voluntary contractions is often used as a proxy for muscle force (Hagberg  
98 et al., 1985; Ueda et al., 1998; Farella et al., 2009). When maximum muscle forces are estimated  
99 from muscle PCSAs, the normalised levels of EMG activity can be used to scale the force  
100 magnitudes produced under a certain task (see Ross et al. 2005 for a study in *Macaca*). This  
101 approach is limited to superficial muscles unless invasive methods are used (Soderberg and  
102 Cook, 1984; Reaz et al., 2006), which constrains its use in living humans. Although the EMG  
103 activity of masticatory muscles has a complex relationship with bite force, during isometric  
104 contraction a close-to-linear relationship is found (Prum et al., 1978; Hagberg et al., 1985;  
105 Wang et al., 2000). During biting tasks, a symmetric pattern of activation has been observed  
106 during maximum intercuspitation (Ferrario et al., 2000; Schindler et al., 2005), unilateral food  
107 crushing (Spencer, 1998) and isometric bites (van Eijden, 1990) but not during complete,  
108 consecutive mastication cycles (Stohler, 1986). Additionally, Farella et al. (2009) found  
109 changing patterns of muscle activation over time under maximum and sub-maximum

110 sustained unilateral bites. Intra and inter-individual variability in muscle force levels is then an  
111 additional source of complexity in data reproduction.

112 The effects of incorrectly reproducing the magnitudes of masticatory muscle forces on  
113 reaction forces and the mode and magnitude of deformation predicted by FE models of the  
114 human cranium have not yet been explored, and is the aim of the present study. Deformation  
115 is assessed both locally using strains and globally (i.e. general changes in size and shape) using  
116 geometric morphometric methods (Fitton et al., 2012; O'Higgins and Milne, 2013).

117 We tested the hypothesis that varying the relative magnitudes of muscle force during the same  
118 biting task has no effect on FEA results in terms of strain distribution and magnitudes, bite  
119 forces, TMJ reaction forces and global modes of model deformation. To test this hypothesis,  
120 several extreme combinations of muscle forces representing different patterns of muscle  
121 activation were simulated while skull and muscle anatomy, tissue material properties and the  
122 kinematic constraints of the model were kept constant. It is to be expected from Hooke's law  
123 that principal strain magnitudes will scale linearly with applied total load (O'Higgins and Milne,  
124 2013), however the expectations with regard to modes of deformation are less clear.

125

126 Materials and Methods

127 Data

128 An FE model of the cranium of a male human aged 43, with full dentition, was built from  
129 segmented CT data used in previous studies (Toro-Ibacache et al., 2015a; Toro-Ibacache et al.,  
130 2015b), where muscle CSAs were also directly measured. The image data comprise a medical  
131 CT scan of a living patient taken at the Teaching Hospital of the University of Chile (Hospital  
132 Clínico de la Universidad de Chile, Santiago de Chile). The data were used with ethics  
133 committee approval, under the terms of the hospital ethics protocol for the use of patient data.  
134 The CT scan was carried out for medical reasons before the beginning of this study using a  
135 Siemens 64-channel multidetector CT scanner equipped with a STRATON tube (Siemens  
136 Somatom Sensation 64, Siemens Healthcare, Erlangen, Germany). The primary reconstruction  
137 of images was performed using specialist software tool (Syngo Multimodality Workplace,  
138 Siemens Healthcare, Erlangen, Germany). Voxel size was 0.44 x 0.44 x 1 mm. The  
139 segmentation was performed on the image stacks exported as DICOM files.

140 Three-dimensional cranial morphology was reconstructed from the CT volume stack using  
141 Avizo (v.7.0.1, Visualization Sciences Group, Burlington, USA). Semi-automated segmentation  
142 of CTs based on grey level thresholds was used to separate bone from surrounding tissues and  
143 air. Manual segmentation was then performed where needed for anatomical accuracy.  
144 Paranasal sinuses were preserved but cortical and cancellous bone were not segmented as  
145 distinct tissues, rather the bone was treated as a solid whole with the material properties of  
146 cortical bone. This approach has been used in a macaque model (Fitton et al., 2015) and  
147 validated in a previous study (Toro Ibacache, 2014) that showed little effect on mode of  
148 deformation (the key focus of this study).

#### 149 Finite element model and loadcases

150 The volume data produced by the CT segmentation was resampled to an isometric voxel size  
151 of 0.44 mm, exported as BMP stacks and converted into an FE mesh of 6,306,181 eight-noded  
152 cubic elements by direct voxel conversion. Cancellous bone was omitted, and hence all bone  
153 was modelled as a solid material with a Young's modulus of 17 GPa and 50 GPa for teeth,  
154 both with a Poisson's ratio of 0.3. This model building approach has been used in previous  
155 studies of cranial FE models (Wroe et al., 2010; Bright and Gröning, 2011; Fitton et al., 2012;  
156 Jansen van Rensburg et al., 2012; Toro-Ibacache et al., 2015b) and is relevant in cases where  
157 model resolution, fossilization or taphonomic processes do not allow to accurately model  
158 cancellous bone (Bright and Gröning, 2011; Fitton et al., 2015; Toro-Ibacache et al., 2015b), or  
159 when models are generated via 3D surface warping (O'Higgins et al., 2011).

160 Each loaded model was kinematically constrained at the most anterior and superior parts of  
161 both mandibular fossae in the x, y and z axes. Vertical constraints on the incisal border of both  
162 central incisors ( $I^1$ ) and on the occlusal face of left and right first molars ( $M^1$ ) were applied  
163 separately, simulating bite points. The choice of axes of constraint was based on prior  
164 experiments in which constraints were reduced (e.g. TMJ constrained in x and y only) with the  
165 result that the model experienced rigid-body motion when loaded. Thus the chosen constraints  
166 were the minimum required to fix the model in space while not over-constraining it. Left and  
167 right  $M^1$  bites were simulated to control for possible effects of asymmetries in bone  
168 morphology and muscle attachment. Muscle origins and insertions were reproduced in the  
169 model based on the original CT image in which muscles were clearly visible.

170

171 Muscle forces

172 Static bites were simulated at I<sup>1</sup> and unilaterally at the left or right M<sup>1</sup>. As noted above, the  
173 maximum muscle forces from the temporal, masseter and medial pterygoid muscles were  
174 estimated from their CSAs measured in previous studies (Toro-Ibacache et al., 2015a; Toro-  
175 Ibacache et al., 2015b) using a protocol based on that of Weijs and Hillen (1984) and the  
176 formula, Force = CSA x 37 N/cm<sup>2</sup>, where the last term is an estimate of the magnitude of  
177 intrinsic muscle strength for human masticatory muscles (Weijs and Hillen, 1985; O'Connor et  
178 al., 2005). The estimated values of CSA and maximum forces are presented in Table 1.

179 Before assessing the impact of different loading scenarios on FE model performance, two  
180 sensitivity analyses were undertaken. In the first, the results of applying maximal forces based  
181 on estimated CSAs, which are asymmetric (Table 1), were compared with identical biting  
182 simulations using symmetric muscle forces (average of left and right applied to both sides). In  
183 the second, the strain maps resulting from the simulated bites on left and right M1 were  
184 compared to check that bites on different sides produce results that are approximately  
185 reflected versions of each other.

186 To test the hypothesis, loadcases simulating different muscle activation levels for each bite  
187 point were made by scaling the estimated maximum muscle forces (Ross et al., 2005; Fitton et  
188 al., 2012). Since it is impractical to reproduce all possible combinations of muscle forces, three  
189 main patterns of 'activation' were explored, based on EMG studies of individuals performing  
190 different biting tasks. These simulated activation patterns use: symmetric and homogeneously  
191 activated muscles during I<sup>1</sup> and unilateral M<sup>1</sup> bites, asymmetric and homogeneously activated  
192 muscles during unilateral M<sup>1</sup> bites and symmetric and asymmetric heterogeneously activated  
193 muscles under both I<sup>1</sup> and M<sup>1</sup> bites.

194 To simulate symmetric, homogeneous muscle activations (van Eijden, 1990; Spencer, 1998),  
195 the models were loaded during both I<sup>1</sup> and M<sup>1</sup> biting simulations with the forces of the three  
196 pairs of jaw-elevator muscles all scaled to 100%, 50% or 25% of maximum force.

197 To simulate asymmetric, homogeneously activated muscles during M<sup>1</sup> biting (Blanksma and van  
198 Eijden, 1995), each muscle of the working side applied 100% of its maximum force. On the  
199 balancing side, the forces applied by each muscle were simultaneously scaled to 75%, 50% or  
200 25% of the maximum.



201 To simulate symmetric, heterogeneously activated muscles (Vitti and Basmajian, 1977; Moore  
202 et al., 1988; van Eijden, 1990; Blanksma and van Eijden, 1995; Farella et al., 2009), during I<sup>1</sup>  
203 biting the maximum forces of the temporalis, masseter and medial pterygoid were applied in  
204 the ratio of 50%:100%:100%, and then 25%:100%:100% of maximum force. In the  
205 asymmetric, heterogeneously activated loadcases during M<sup>1</sup> biting simulations, 50% of the  
206 maximum force of all balancing side muscles was applied. Two separate sets of working side  
207 forces were applied in the following ratios: temporalis:masseter:medial  
208 pterygoid=50%:100%:100% and 25%:100%:100%.

209 Details of muscle activations in each loadcase are provided in Table 2. Loadcases 1 to 3  
210 simulate symmetric, homogeneous muscle activations under I<sup>1</sup> bites. Loadcases 4 to 9 simulate  
211 symmetric, homogeneous activations under left and then right M<sup>1</sup> bites. Loadcases 10 to 15  
212 represent asymmetric, homogeneously activated muscles during left and then right M1 biting.  
213 Loadcases 16 and 17 represent symmetric, heterogeneously activated muscles during I1 biting.  
214 Loadcases 18 to 21 simulate asymmetric, heterogeneously activated loadcases during left and  
215 then right M1 bites.

216 Model pre- and postprocessing were performed using the FEA program VOX-FE (Fagan et  
217 al., 2007; Liu et al., 2012).

218

219 Comparison of mechanical performance among loadcases

220 Bite forces and TMJ reaction forces were calculated by summing the forces predicted by the  
221 FEA at each constrained node on the tooth. Force magnitudes were then plotted against  
222 applied muscle forces to assess the relationships between these variables. Deformation of the  
223 model was assessed by comparing strain contour plots, representing the spatial distribution of  
224 regions of high and low strains and their magnitudes. Global modes of deformation were also  
225 compared among loadcases using Procrustes size and shape analyses based on a configuration  
226 of 51 craniofacial landmarks (Table 3) representing the form of the cranium and facial  
227 structures normally strained during biting (Demes, 1987; Gross et al., 2001; Kupczik et al.,  
228 2009; Ross et al., 2011). The Procrustes size and shape analysis comprises rotation and  
229 translation but not scaling of the landmark coordinates of the original, unloaded cranium and  
230 the coordinates from the deformed, loaded crania, followed by principal components analysis  
231 (PCA) of the new coordinates (Fitton et al., 2012; O'Higgins et al., 2012). It has been argued  
232 (Curtis et al., 2011) that zygomatic arch deformations from primate skull FEA may not  
233 accurately reflect reality because the temporalis fascia which is, as in this study often omitted,  
234 may limit zygomatic arch deformation in life. Therefore, in order to assess the impact of  
235 zygomatic arch deformation on the analysis of global model deformation the size and shape  
236 analysis was repeated using a subset of 43 landmarks, excluding those located in the zygomatic  
237 arch (see Table 3).

238 The analysis of global model deformation was performed using the EVAN toolbox (v.1.62,  
239 [www.evan-society.org](http://www.evan-society.org)).

240

## 241 Results

242 Before considering the results in relation to the hypothesis, two initial sensitivity analyses are  
243 reported. In the first, the results of applying maximum forces based on estimated CSAs, that  
244 are asymmetric (Table 1), are compared with identical biting simulations using identical left-  
245 right muscle forces (average of left and right, applied to both sides). Compared to the  
246 loadcases based on directly estimated (and so, asymmetric) maximum muscle forces, the  
247 symmetric loadcases predicted virtually identical bite forces, TMJ reaction forces and strain  
248 magnitudes. With regard to mode of deformation, patterns of strain distribution (data not  
249 shown) and global model deformation (see results for all loadcases) assessed by landmarks  
250 were also almost identical. In the second sensitivity analysis, bites on left and right M<sup>1</sup> resulted  
251 in strain contour maps that are almost perfect mirror images of each other (data not shown).  
252 As such, only the strain distributions and magnitudes under left M<sup>1</sup> bites are considered  
253 further.

### 254 Strain distribution and magnitudes

255 For each simulated bite, the strain contour maps arising from different loadcases show  
256 differences in strain magnitudes but much less so in distribution. Thus, where strains are  
257 predicted to be relatively high or low differs little among simulations but the average strain  
258 magnitude does differ.

259 The highest strains and largest fields of high strain are found in the regions of masseter and  
260 medial pterygoid attachment, and in the facial regions close to the bite point. That is, during  
261 incisor bites, the maxilla adjacent to the nasal notch and, during molar bites, the zygomatic  
262 region and frontal process of the maxilla (Figs. 1 and 2).

263 During I<sup>1</sup> biting simulations, strains decrease from maximum values of >200  $\mu\epsilon$  to 100-200  $\mu\epsilon$   
264 in the face, zygomatic arch and mandibular fossae as the magnitude of total applied muscle  
265 force decreases. Although this was expected for models 1-3, in the other I<sup>1</sup> loadcases the  
266 distribution of regions of high and low strain hardly varies, irrespective of the pattern of  
267 muscle activation (Fig. 1). The same situation occurs in the face during unilateral M<sup>1</sup> bites. In  
268 the mandibular fossa, strain magnitudes differ between left and right sides among loadcases.  
269 The loadcases with more symmetric total muscle forces, i.e. loadcases 4 to 9 and 18 to 21 (see  
270 Table 2 for details), predict the highest strains over the mandibular fossa of the balancing side

271 relative to the working side (e.g. in loadcase 4, strains in the fossae exceed 200  $\mu\epsilon$  and are larger  
272 on the balancing than on the working side; Fig. 2). This pattern is inverted when the most  
273 markedly asymmetric activation patterns are applied (loadcases 11, 12, 14 and 15; Fig. 2). Thus,  
274 when the most asymmetric muscle activation pattern is applied (loadcases 12 and 15), the  
275 mandibular fossa of the working side shows a larger area reaching strains over 200  $\mu\epsilon$  than the  
276 balancing side fossa where most strains are  $\sim 150 \mu\epsilon$  (Fig. 2).

#### 277 Bite force and TMJ reaction force

278 Predicted bite forces and TMJ reaction forces (Table 2; Figs. 3 to 5) are consistent with the  
279 results depicted by the strain contour plots. In general, bite force and TMJ reaction force  
280 increase in proportion to total applied muscle force, particularly during I<sup>1</sup> bites (loadcases 1 to  
281 3, 16 and 17; Figs. 3a and 5a). During M<sup>1</sup> bites, TMJ reaction force is higher on the balancing  
282 side than the working side with homogeneously activated muscles (loadcases 4 to 9; Figs. 3b  
283 and 3c). In contrast, increasingly asymmetric, homogenous loadcases (10 to 15; Fig. 4) predict  
284 lower TMJ forces on the balancing than the working side, and those with asymmetric,  
285 heterogeneously activated muscles (i.e. those with varying working side temporalis force,  
286 loadcases 18 to 21; Figs. 5b and 5c) further reduce the TMJ force difference between working  
287 and balancing sides.

#### 288 Global model deformation

289 The Procrustes size and shape PCA of cranial deformations resulting from FEA distinguished  
290 three different general vectors of deformation, one for each bite point. These are represented  
291 as lines connecting the unloaded model and the loadcases for each bite point (Fig. 6).  
292 Differences among loadcases with the same bite point comprise mainly of differences in  
293 magnitude (distance from the unloaded model) rather than mode (direction of vector). The  
294 vectors connecting the unloaded and molar biting simulations are almost symmetrically  
295 disposed about the vectors representing incisor bites (Fig. 6). Thus, the global model  
296 deformations arising from left and right M<sup>1</sup> bites are almost mirror images of each other. The  
297 small degree of asymmetry in the vectors likely reflects asymmetry of form. These findings  
298 reflect the symmetries and asymmetries of the strain contour maps noted earlier.

299 The largest degrees of deformation (distances between unloaded and loaded models in the  
300 plot) are achieved when muscles are activated homogeneously and maximally, irrespective of

301 the bite point. Examining the inset warpings, in both I<sup>1</sup> and M<sup>1</sup> bites the greatest deformations  
302 occur in the alveolar process near the bite point. With incisor bites the lower face is dorso-  
303 ventrally deflected with respect to the upper face and neurocranium. With M<sup>1</sup> bites the face  
304 undergoes torsion and local deformation above the bite point. The vectors of deformation of  
305 the models with symmetrically applied but varying muscle forces scale exactly in proportion to  
306 applied force and are coincident in direction. As noted earlier for strains, loadcases created  
307 using perfectly symmetric muscle forces (the average of left and right) deform along almost  
308 identical vectors as models using their directly estimated and so, asymmetric force magnitudes  
309 (loadcases 1S to 9S, Fig. 6).

310 The omission of zygomatic arch landmarks has a small effect on the PCA of FEA results (Fig.  
311 7). The main effect is that the vectors from all muscle activation patterns applied to each bite  
312 point more nearly overlap. This indicates that deformations of the zygomatic arch accounted  
313 for a substantial portion of the divergences between vectors representing the same bite point  
314 in Fig. 6.

315

316 Discussion

317 The present study assessed the effects on FE model performance of varying muscle activations  
318 during simulated static incisor and molar bites. This is important because muscle forces are  
319 rarely known with any precision, and this is especially so when simulating biting in fossil or  
320 skeletal material. In consequence, simplified or estimated loadings are often applied. Thus  
321 maximal muscle forces might be more or less accurately estimated from bony proxies (Wroe et  
322 al., 2010) or estimated from data corresponding to other, related species (Strait et al., 2009;  
323 Smith et al., 2015b). Forces might be applied to simulate maximum (100%) activation of all  
324 muscles (Smith et al., 2015a) or some more complex muscle activation pattern might be used  
325 (Kupczik et al., 2009). This study aimed to assess the sensitivity of some aspects of FE model  
326 performance to such variations in muscle activations; namely strains, bite forces, TMJ forces  
327 and global modes of model deformation.

328 The null hypothesis is that varying the relative magnitudes of muscle force during the same  
329 biting task has no effect on FEA results in terms of strain distribution and magnitudes, bite  
330 forces, TMJ reaction forces and global modes of model deformation. Strictly, this hypothesis  
331 was falsified, but the effects of varying muscle activation pattern on modes of deformation are  
332 very small everywhere except in the zygomatic arch and mandibular fossa. As expected given  
333 that bone is represented by an isotropic linearly elastic material, the effect of varying  
334 magnitudes of force is to proportionately diminish the magnitude of model deformation.  
335 Likewise, bite and TMJ reaction forces also scale with muscle force. These results are further  
336 discussed below.

337 Strain distribution and magnitude

338 During all simulations, strains are greatest in the in the vicinity of the bite point and large  
339 where the masseter and medial pterygoid muscles attach. Temporalis, in having a very large  
340 attachment area to the large, stiff cranium, does not produce large strains over the vault when  
341 it contracts. Thus the major changes in cranial strain maps between muscle activation patterns  
342 occur in the regions of the masseter and medial pterygoid attachments.

343 The results of this study indicate that the greatest impact on facial strains arises through  
344 variations in the total applied muscle force. Strain magnitudes (Figs. 1 and 2) show an  
345 approximately linear relationship with total applied muscle force. This is in agreement with the

346 results of Ross et al. (2005) and Fitton et al. (2012) in macaque models and it is expected for  
347 linearly elastic materials.

348 Varying simulated muscle activation patterns has a small impact on strain distribution.  
349 Principally this affects the regions local to the masseter muscle attachment site, causing strains  
350 to vary in this region according to the force of masseter contraction. This finding of consistent  
351 strain distribution under different muscle loading regimens points to the possibility of  
352 performing reliable FEAs of living, archaeological and fossil hominin crania using simplified  
353 muscle activations (e.g. symmetrically applied maximal muscle forces). Estimates of these  
354 forces might be obtained from the literature, directly from muscle CSAs as in the present  
355 study, or from bony proxies. This last method of estimation is likely to be inaccurate (Antón,  
356 1994; Toro-Ibacache et al., 2015a). However, such inaccuracy likely will impact strain  
357 magnitudes but not relative facial strains. Thus, if relative rather than absolute strains are of  
358 interest, reasonable muscle activation patterns all produce approximately similar results insofar  
359 as they apply similar total force.

360 The present study varied relative force magnitudes but not muscle orientations. Each muscle  
361 was considered to have a single vector of action. This was a necessary simplification given the  
362 resolution of the CT images, since the finer details of muscle anatomy and fibre directions are  
363 not known. It is worth noting in this regard that subdividing e.g. the masseter into different  
364 parts with different vectors may introduce significant errors in estimation of the principal  
365 vector of muscle action (Röhrle and Pullan, 2007). The effect of varying the directions of  
366 muscle force vectors is worth exploring in future studies, especially where only the cranium is  
367 available and the position of mandibular muscle insertions has to be estimated. It is likely that  
368 such variations of vectors will principally impact modes of deformation.

369 Bite force and TMJ reaction force

370 As expected with strain magnitudes, predicted bite force is proportional to total applied muscle  
371 force (Table 3). The same occurs with TMJ reaction forces during I<sup>1</sup> bites. During I<sup>1</sup> biting,  
372 small asymmetries in TMJ reaction forces can be observed, which is expected given the normal  
373 asymmetry of the skull.

374 Temporomandibular joint loading is an important human masticatory functional parameter;  
375 altered load distribution during mastication may result in dysfunction due to morphological  
376 changes and an inflammatory response in the articular tissues (McNamara, 1975; Tanaka et al.,

377 2008; Barton, 2012). Temporomandibular joint loading in humans is difficult to estimate due  
378 to the impracticability of using direct methods and also because the mathematical models used  
379 to predict it have been shown to be highly sensitive to variations in muscle parameters  
380 (Throckmorton, 1985; Koolstra et al., 1988). Nevertheless, today it is generally acknowledged  
381 that during unilateral bites, the TMJ of the balancing side is more loaded than that of working  
382 side (Hylander, 1975; Throckmorton and Throckmorton, 1985; Koolstra and van Eijden, 2005;  
383 Shi et al., 2012). In this study such differences in loading between working and balancing sides  
384 are achieved during symmetric or close to symmetric muscle activations. However, under  
385 unilateral bites a much greater asymmetry (irrespective of heterogeneity) in muscle activations  
386 reverses the relationship between TMJ reaction forces at the working and balancing sides (Fig.  
387 3). The sensitivity of TMJ reaction forces in the FE model to asymmetries in simulated muscle  
388 activations calls for further investigation using e.g. multibody dynamic approaches (Curtis,  
389 2011; Shi et al., 2012) to better understand the apparent reversal of TMJ reaction forces.

390 Considering these results, symmetrical maximum muscle forces appear to be a reasonable  
391 simplification approach in FEAs of the human cranium as long as relative rather than absolute  
392 strain magnitudes are of interest.

### 393 Global model deformation

394 As with predicted strains and bite forces, for each simulated bite point, varying the muscle  
395 activation pattern mainly produces differences in the magnitude rather than mode of global  
396 model deformation of the cranium as assessed by PCA of size and shape coordinates. This  
397 magnitude relates to the total applied muscle force and reflects the linear relationship between  
398 load and deformation in isotropic linear elastic materials (as bone and teeth are modelled here),  
399 and is consistent with the findings of O'Higgins and Milne (2013) in femora.

400 That asymmetric muscle activations principally impact on zygomatic arch deformation is  
401 consistent with the findings of Fitton et al. (2012) who also noted that varying muscle  
402 activations mainly led to differences in the degree of zygomatic arch deformation. Principally  
403 this affects the regions local to the masseter muscle attachment site. We found that ignoring  
404 zygomatic landmarks in the size and shape analysis results in vectors of deformation that  
405 closely overlap for each bite point, irrespective of muscle activation pattern. This may reflect a  
406 physiological, greater sensitivity of the zygomatic region to varying muscle force or it may be a  
407 consequence of inadequate representation of the temporal fascia (Curtis et al., 2011). The



408 present study is uninformative in this regard. However, removing zygomatic arch landmarks  
409 does not affect the way model deformation in the face is depicted: dorsal bending of the  
410 maxilla during I<sup>1</sup> bites and apical-buccal deformation of the tooth and its alveolar bone during  
411 M<sup>1</sup> bites.

412

413

414 Conclusion

415 The results of this study show that the main effect of varying relative magnitudes of applied  
416 muscle forces on the FE model of a human cranium during simulated biting concerns the  
417 scaling of deformation (local strains and global size and shape change) and bite force with total  
418 applied muscle force. The effect on mode of deformation is much smaller, principally  
419 impacting on the zygomatic arch, where masseter attaches. TMJ reaction forces seem to be  
420 sensitive to symmetry of loading of the masticatory system

421 The hypothesis that varying the relative magnitudes of muscle forces during the same biting  
422 task has no effect on FEA results in terms of strain distribution and magnitude, bite force,  
423 TMJ reaction force and global model deformation was falsified. Thus, while modes of  
424 deformation (as assessed by strain distributions and the size and shape PCA) are relatively  
425 unaltered, the magnitudes of deformation vary with total applied muscle force as might be  
426 expected. Likewise, and as expected, bite force covaries with total applied muscle force. On the  
427 other hand, the relative magnitudes of left and right TMJ reaction forces are sensitive to  
428 applied muscle forces, especially asymmetry of these forces.

429 Considering these findings, when relative strain magnitudes among cranial regions are the  
430 focus of interest, the use of symmetric maximum muscle forces is a reasonable loading  
431 simplification. However the degree of deformation and so, magnitudes of strains are unlikely  
432 to be accurately predicted unless accurate muscle forces are applied. This is of particular  
433 relevance in the study of archaeological material and fossil hominins, where no muscle data are  
434 available.

435

436 Acknowledgments

437 The authors would like to thank Hospital Clínico Universidad de Chile (Chile) and Víctor  
438 Zapata Muñoz for support in early stages of data collection. We are also thankful to Sam Cobb  
439 and Laura Fitton (Hull York Medical School, UK), Catarina Hagberg (Karolinska Institutet,  
440 Sweden), Kornelius Kupczik (Max Planck Weizmann Center for Integrative Archaeology and  
441 Anthropology, Germany) and Rodolfo Miralles (Universidad de Chile, Chile) for helpful  
442 comments and discussion during different stages of this work. VT-I was funded by Becas  
443 Chile-CONICYT Grant (Comisión Nacional de Investigación Científica y Tecnológica, Chile).

444 References

- 445 Antón SC. 1990. Neandertals and the anterior dental loading hypothesis: A biomechanical  
446 evaluation of bite force production. *Kroeber Anthropol Soc Pap* 71-72:67-76.
- 447 Antón SC. 1994. Masticatory muscle architecture and bone morphology in primates. In.  
448 Berkeley: University of California.
- 449 Antón SC. 1999. Macaque masseter muscle: internal architecture, fiber length and cross-  
450 sectional area. *Int J Primatol* 20:441-462.
- 451 Barton ER. 2012. Mechanical signal transduction: divergent communication and the potential  
452 consequences for masticatory muscle. *Semin Orthod* 18:2-9.
- 453 Blanksma N, van Eijden T. 1995. Electromyographic heterogeneity in the human temporalis  
454 and masseter muscles during static biting, open\ close excursions, and chewing. *J Dent*  
455 *Res* 74:1318-1327.
- 456 Bright JA. 2012. The Importance of Craniofacial Sutures in Biomechanical Finite Element  
457 Models of the Domestic Pig. *PLoS ONE* 7:e31769.
- 458 Bright JA, Gröning F. 2011. Strain accommodation in the zygomatic arch of the pig: a  
459 validation study using digital speckle pattern interferometry and finite element analysis.  
460 *J Morphol* 272:1388-1398.
- 461 Curtis N. 2011. Craniofacial biomechanics: an overview of recent multibody modelling studies.  
462 *J Anat* 218:16-25.
- 463 Curtis N, Witzel U, Fitton LC, O'higgins P, Fagan MJ. 2011. The mechanical significance of  
464 the temporal fasciae in *Macaca fascicularis*: an investigation using finite element analysis.  
465 *Anat Rec* 294:1178-1190.
- 466 Demes B. 1987. Another look at an old face: biomechanics of the Neandertal facial skeleton  
467 reconsidered. *J Hum Evol* 16:297-303.
- 468 Demes B, Creel N. 1988. Bite force, diet, and cranial morphology of fossil hominids. *J Hum*  
469 *Evol* 17:657-670.
- 470 Fagan MJ, Curtis N, Dobson CA, Karunanayaje JH, Kupczik K, Moazen M, Page L, Phillips R,  
471 O'Higgins P. 2007. Voxel-based finite analysis - Working directly with MicroCT scan  
472 data. *J Morphol* 268:1071.

473 Farella M, Palumbo A, Milani S, Avecone S, Gallo L, Michelotti A. 2009. Synergist coactivation  
474 and substitution pattern of the human masseter and temporalis muscles during  
475 sustained static contractions. Clin Neurophysiol 120:190-197.

476 Ferrario V, Sforza C, Colombo A, Ciusa V. 2000. An electromyographic investigation of  
477 masticatory muscles symmetry in normo-occlusion subjects. J Oral Rehabil 27:33-40.

478 Fitton LC, Prôa M, Rowland C, Toro-Ibacache V, O'Higgins P. 2015. The impact of  
479 simplifications on the performance of a finite element model of a *Macaca fascicularis*  
480 cranium. Anat Rec 298:107-121.

481 Fitton LC, Shi JF, Fagan MJ, O'Higgins P. 2012. Masticatory loadings and cranial deformation  
482 in *Macaca fascicularis*: a finite element analysis sensitivity study. J Anat 221:55-68.

483 Gröning F, Fagan M, O'Higgins P. 2011. The effects of the periodontal ligament on  
484 mandibular stiffness: a study combining finite element analysis and geometric  
485 morphometrics. J Biomech 44:1304-1312.

486 Gross MD, Arbel G, Hershkovitz I. 2001. Three-dimensional finite element analysis of the  
487 facial skeleton on simulated occlusal loading. J Oral Rehabil 28:684-694.

488 Hagberg C, Agerberg G, Hagberg M. 1985. Regression analysis of electromyographic activity  
489 of masticatory muscles versus bite force. Eur J Oral Sci 93:396-402.

490 Hylander WL. 1975. The human mandible: lever or link? Am J Phys Anthropol 43:227-242.

491 Jansen van Rensburg GJ, Wilke DN, Kok S. 2012. Human skull shape and masticatory induced  
492 stress: Objective comparison through the use of non-rigid registration. Int J Numer  
493 Method Biomed Eng 28:170-185.

494 Koolstra J, Tanaka E. 2009. Tensile stress patterns predicted in the articular disc of the human  
495 temporomandibular joint. J Anat 215:411-416.

496 Koolstra J, van Eijden T. 2005. Combined finite-element and rigid-body analysis of human jaw  
497 joint dynamics. J Biomech 38:2431-2439.

498 Koolstra J, van Eijden T, Weijs W, Naeije M. 1988. A three-dimensional mathematical model  
499 of the human masticatory system predicting maximum possible bite forces. J Biomech  
500 21:563-576.

501 Kupczik K. 2008. Virtual biomechanics: basic concepts and technical aspects of finite element  
502 analysis in vertebrate morphology. J Anthropol Sci 86:193-198.

503 Kupczik K, Dobson CA, Crompton RH, Phillips R, Oxnard CE, Fagan MJ, O'Higgins P.  
504 2009. Masticatory loading and bone adaptation in the supraorbital torus of developing  
505 macaques. *Am J Phys Anthropol* 139:193-203.

506 Kupczik K, Dobson CA, Fagan MJ, Crompton RH, Oxnard CE, O'Higgins P. 2007. Assessing  
507 mechanical function of the zygomatic region in macaques: validation and sensitivity  
508 testing of finite element models. *J Anat* 210:41-53.

509 Liu J, Shi J, Fitton LC, Phillips R, O'Higgins P, Fagan MJ. 2012. The application of muscle  
510 wrapping to voxel-based finite element models of skeletal structures. *Biomech Model*  
511 *Mechan* 11:35-47.

512 McNamara J. 1975. Functional adaptations in the temporomandibular joint. *Dent Clin N Am*  
513 19:457.

514 Moore CA, Smith A, Ringel RL. 1988. Task-specific organization of activity in human jaw  
515 muscles. *J Speech Lang Hear R* 31:670.

516 O'Connor CF, Franciscus RG, Holton NE. 2005. Bite force production capability and  
517 efficiency in Neandertals and modern humans. *Am J Phys Anthropol* 127:129-151.

518 O'Higgins P, Cobb SN, Fitton LC, Gröning F, Phillips R, Liu J, Fagan MJ. 2011. Combining  
519 geometric morphometrics and functional simulation: an emerging toolkit for virtual  
520 functional analyses. *J Anat* 218:3-15.

521 O'Higgins P, Fitton LC, Phillips R, Shi J, Liu J, Gröning F, Cobb SN, Fagan MJ. 2012. Virtual  
522 functional morphology: novel approaches to the study of craniofacial form and  
523 function. *Evol Biol* 39:521-535.

524 O'Higgins P, Milne N. 2013. Applying geometric morphometrics to compare changes in size  
525 and shape arising from finite elements analyses. *Hystrix* 24:126-132.

526 Prum G, Ten Bosch J, De Jongh H. 1978. Jaw muscle EMG-activity and static loading of the  
527 mandible. *J Biomech* 11:389-395.

528 Rayfield EJ. 2007. Finite element analysis and understanding the biomechanics and evolution  
529 of living and fossil organisms. *Annu Rev Earth Planet Sci* 35:541-576.

530 Reaz MB, Hussain M, Mohd-Yasin F. 2006. Techniques of EMG signal analysis: detection,  
531 processing, classification and applications. *Biol Proced Online* 8:11-35.

532 Richmond BG, Wright BW, Grosse I, Dechow PC, Ross CF, Spencer MA, Strait DS. 2005.  
533 Finite element analysis in functional morphology. *Anat Rec* 283:259-274.

534 Ross CF, Berthaume MA, Dechow PC, Iriarte-Diaz J, Porro LB, Richmond BG, Spencer M,  
535 Strait D. 2011. *In vivo* bone strain and finite-element modeling of the craniofacial haft  
536 in catarrhine primates. *J Anat* 218:112-141.

537 Ross CF, Patel BA, Slice DE, Strait DS, Dechow PC, Richmond BG, Spencer MA. 2005.  
538 Modeling masticatory muscle force in finite element analysis: sensitivity analysis using  
539 principal coordinates analysis. *Anat Rec* 283:288-299.

540 Schindler HJ, Rues S, Türp JC, Schweizerhof K, Lenz J. 2005. Activity patterns of the  
541 masticatory muscles during feedback-controlled simulated clenching activities. *Eur J*  
542 *Oral Sci* 113:469-478.

543 Shi J, Curtis N, Fitton LC, O'Higgins P, Fagan MJ. 2012. Developing a musculoskeletal model  
544 of the primate skull: Predicting muscle activations, bite force, and joint reaction forces  
545 using multibody dynamics analysis and advanced optimisation methods. *J Theor Biol*  
546 310:21-30.

547 Smith AL, Benazzi S, Ledogar JA, Tamvada K, Pryor Smith LC, Weber GW, Spencer MA,  
548 Dechow PC, Grosse IR, Ross CF, Richmond BG, Wright BW, Wang Q, Byron C, Slice  
549 DE, Strait DS. 2015a. Biomechanical Implications of Intraspecific Shape Variation in  
550 Chimpanzee Crania: Moving Toward an Integration of Geometric Morphometrics and  
551 Finite Element Analysis. *Anat Rec* 298:122-144.

552 Smith AL, Benazzi S, Ledogar JA, Tamvada K, Pryor Smith LC, Weber GW, Spencer MA,  
553 Lucas PW, Michael S, Shekeban A, Al-Fadhalah K, Almusallam AS, Dechow PC,  
554 Grosse IR, Ross CF, Madden RH, Richmond BG, Wright BW, Wang Q, Byron C,  
555 Slice DE, Wood S, Dzialo C, Berthaume MA, van Casteren A, Strait DS. 2015b. The  
556 Feeding Biomechanics and Dietary Ecology of *Paranthropus boisei*. *Anat Rec* 298:145-  
557 167.

558 Soderberg GL, Cook TM. 1984. Electromyography in biomechanics. *PhysTher* 64:1813-1820.

559 Spencer MA. 1998. Force production in the primate masticatory system: electromyographic  
560 tests of biomechanical hypotheses. *J Hum Evol* 34:25-54.

561 Stohler C. 1986. A comparative electromyographic and kinesigraphic study of deliberate and  
562 habitual mastication in man. *Arch Oral Biol* 31:669-678.

563 Strait DS, Wang Q, Dechow PC, Ross CF, Richmond BG, Spencer MA, Patel BA. 2005.  
564 Modeling elastic properties in finite-element analysis: How much precision is needed to  
565 produce an accurate model? *Anat Rec* 283:275-287.

566 Strait DS, Weber GW, Neubauer S, Chalk J, Richmond BG, Lucas PW, Spencer MA, Schrein  
567 C, Dechow PC, Ross CF. 2009. The feeding biomechanics and dietary ecology of  
568 *Australopithecus africanus*. PNAS 106:2124-2129.

569 Tanaka E, Detamore M, Mercuri L. 2008. Degenerative disorders of the temporomandibular  
570 joint: etiology, diagnosis, and treatment J Dent Res 87:296-307.

571 Tanne K, Miyasaka J, Yamagata Y, Sachdeva R, Tsutsumi S, Sakuda M. 1988. Three-  
572 dimensional model of the human craniofacial skeleton: method and preliminary results  
573 using finite element analysis. J Biomed Eng 10:246-252.

574 Throckmorton GS. 1985. Quantitative calculations of temporomandibular joint reaction  
575 forces—II. The importance of the direction of the jaw muscle forces. J Biomech  
576 18:453-461.

577 Throckmorton GS, Throckmorton LS. 1985. Quantitative calculations of temporomandibular  
578 joint reaction forces—I. The importance of the magnitude of the jaw muscle forces. J  
579 Biomech 18:445-452.

580 Toro-Ibacache V, Zapata Muñoz V, O'Higgins P. 2015a. The predictability from skull  
581 morphology of temporalis and masseter muscle cross-sectional areas in humans. Anat  
582 Rec:DOI: 10.1002/ar.23156.

583 Toro-Ibacache V, Zapata Muñoz V, O'Higgins P. 2015b. The relationship between skull  
584 morphology, masticatory muscle force and cranial skeletal deformation during biting.  
585 Ann Anat:DOI: 10.1016/j.aanat.2015.1003.1002.

586 Toro Ibacache MV. 2014. A finite element study of the human cranium; the impact of  
587 morphological variation on biting performance. In. York: The University of Hull and  
588 the University of York.

589 Ueda HM, Ishizuka Y, Miyamoto K, Morimoto N, Tanne K. 1998. Relationship between  
590 masticatory muscle activity and vertical craniofacial morphology. Angle Orthod 68:233-  
591 238.

592 van Eijden T. 1990. Jaw muscle activity in relation to the direction and point of application of  
593 bite force. J Dent Res 69:901-905.

594 van Eijden T, Korfage J, Brugman P. 1997. Architecture of the human jaw-closing and jaw-  
595 opening muscles. Anat Rec 248:464-474.

596 van Spronsen P, Weijs W, Valk J, Prahl-Andersen B, van Ginkel F. 1991. Relationships  
597 between jaw muscle cross-sections and craniofacial morphology in normal adults,  
598 studied with magnetic resonance imaging. *Eur J Orthod* 13:351-361.

599 Vitti M, Basmajian JV. 1977. Integrated actions of masticatory muscles: simultaneous EMG  
600 from eight intramuscular electrodes. *Anat Rec* 187:173-189.

601 Wang K, Arima T, Arendt-Nielsen L, Svensson P. 2000. EMG–force relationships are  
602 influenced by experimental jaw-muscle pain. *J Oral Rehabil* 27:394-402.

603 Weijs W, Hillen B. 1984. Relationship between the physiological cross-section of the human  
604 jaw muscles and their cross-sectional area in computer tomograms. *Acta Anat* 118:129-  
605 138.

606 Weijs W, Hillen B. 1985. Cross-sectional areas and estimated intrinsic strength of the human  
607 jaw muscles. *Acta Morphol Neer Sc* 23:267-274.

608 Weijs W, Hillen B. 1986. Correlations between the cross-sectional area of the jaw muscles and  
609 craniofacial size and shape. *Am J Phys Anthropol* 70:423-431.

610 Wood SA, Strait DS, Dumont ER, Ross CF, Grosse IR. 2011. The effects of modeling  
611 simplifications on craniofacial finite element models: The alveoli (tooth sockets) and  
612 periodontal ligaments. *J Biomech* 44:1831-1838.

613 Wroe S, Ferrara TL, McHenry CR, Curnoe D, Chamoli U. 2010. The craniomandibular  
614 mechanics of being human. *Proc R Soc B* 277:3579-3586.

615



616 Figure Legends

617 Figure 1. Strain contour plots from example I<sup>1</sup> biting simulations. The charts depict the  
618 percentages of maximal muscle force applied in each loadcase: working side, dark green bars;  
619 balancing side, light green bars. Loadcases 1, 2 and 3 correspond to symmetric, homogeneous  
620 muscle forces. Loadcases 16 and 17 simulate symmetric, heterogeneous muscle forces, with  
621 lower levels of activation of the temporalis (T) compared to masseter (M) and medial pterygoid  
622 (MP) muscles.

623 Figure 2. Strain contour plots from left M<sup>1</sup> biting simulations. The charts depict the  
624 percentages of maximal muscle force applied in each loadcase: working side, dark green bars;  
625 balancing side, light green bars. Loadcases 4, 5 and 6 correspond to symmetric, homogeneous  
626 muscle forces. Loadcases 10, 11 and 12 correspond to asymmetric, homogeneous muscle  
627 forces, with diminishing simulated activation of balancing side muscles. Loadcases 18 and 19  
628 simulate asymmetric, heterogeneous muscle forces, with the temporalis (T) activated to lesser  
629 degree than masseter (M) and medial pterygoid (MP) muscles on the working side.

630 Figure 3. Bite forces and TMJ reaction forces in loadcases simulating symmetrically and  
631 homogeneously activated muscles. Loadcase number is shown in bold. (a) I<sup>1</sup> bites, (b) left M<sup>1</sup>  
632 bites (working side=left), and (c) right M<sup>1</sup> bites (working side=right).

633 Figure 4. Bite forces and TMJ reaction forces in loadcases simulating asymmetric,  
634 homogeneously activated muscles. Loadcase number is shown in bold. (a) Left M<sup>1</sup> bite  
635 (working side=left), (b) right M<sup>1</sup> bite (working side=right).

636 Figure 5. Loadcases simulating heterogeneously activated muscles. Bite forces and TMJ  
637 reaction forces are plotted against the percentage of maximum temporalis force acting on the  
638 working side. Loadcase number is shown in bold. (a) I<sup>1</sup> bites, (b) left M<sup>1</sup> bites (working  
639 side=left), and (c) right M<sup>1</sup> bites (working side=right).

640 Figure 6. Principal components analysis of 51 cranial landmarks on the unloaded model and  
641 the same model under different loadcases. The lines represent the vectors of deformation  
642 under each loading regimen. Loadcase numbers are shown in bold. S=loadcases with  
643 symmetric muscle force magnitudes, L=left and R=right. The inset surfaces with overlain  
644 transformation grids show: leftmost, the unloaded model; right upper, the largest deformation

645 of the model resulting from right M<sup>1</sup> biting; right middle, the largest deformation resulting  
646 from I<sup>1</sup> biting; right lower, the largest deformation of the model resulting from left M<sup>1</sup> biting,  
647 all with the degree of deformation magnified 1000 times for visualisation.

648 Figure 7. Principal components analysis of 43 cranial landmarks on the unloaded model and  
649 the same model under different loadcases. Landmarks on the zygomatic arch are not included.  
650 The lines represent the vectors of deformation under each loading regimen. Loadcase numbers  
651 are shown in bold. S=loadcases with symmetric muscle force magnitudes, L=left and R=right.  
652 The inset surfaces with overlain transformation grids show: leftmost, the unloaded model;  
653 right upper, the largest deformation of the model resulting from left M<sup>1</sup> biting; right middle,  
654 the largest deformation resulting from I<sup>1</sup> biting; right lower, the largest deformation of the  
655 model resulting from right M<sup>1</sup> biting, all with the degree of deformation magnified 1000 times  
656 for visualisation.

Table 1. Estimated values of CSA and maximum forces of jaw-elevator muscles.

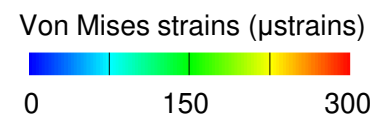
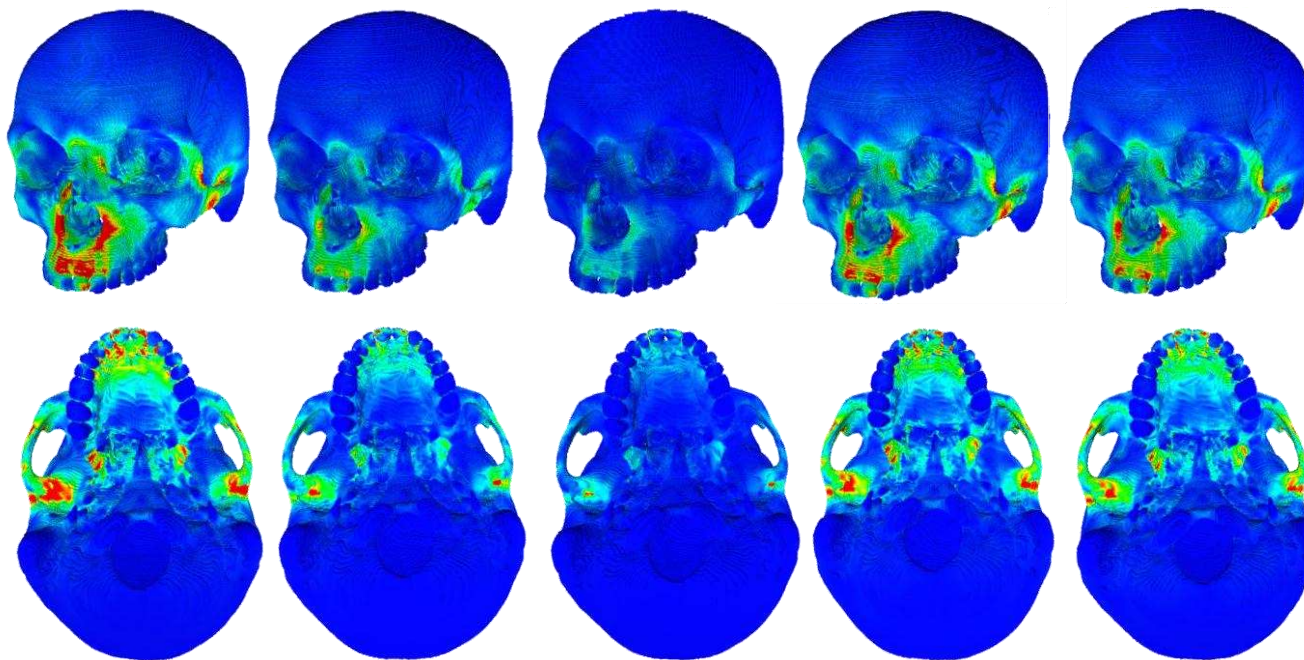
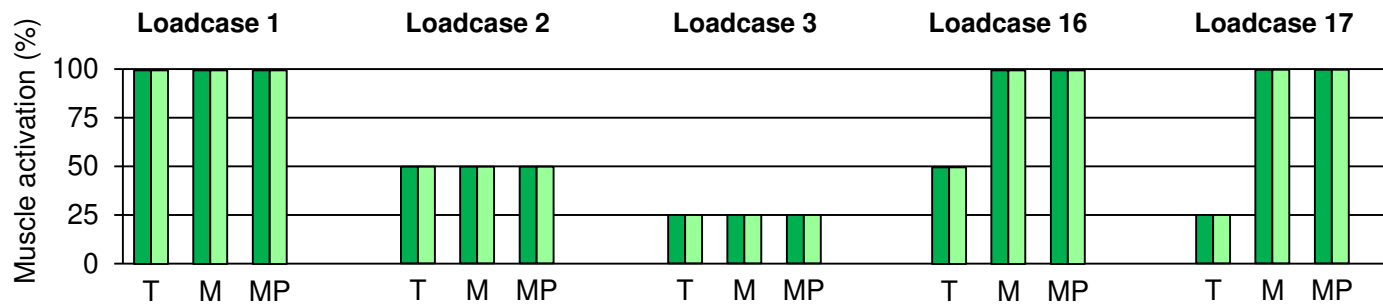
Muscle	CSA (cm <sup>2</sup> )		Muscle force (N)	
	Left	Right	Left	Right
Temporalis	4.54	4.61	168.02	170.67
Masseter	3.62	3.35	134.06	124.01
Medial Pterygoid	3.35	3.18	124.01	117.49

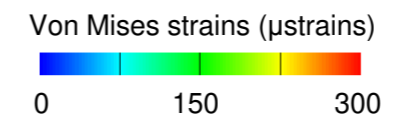
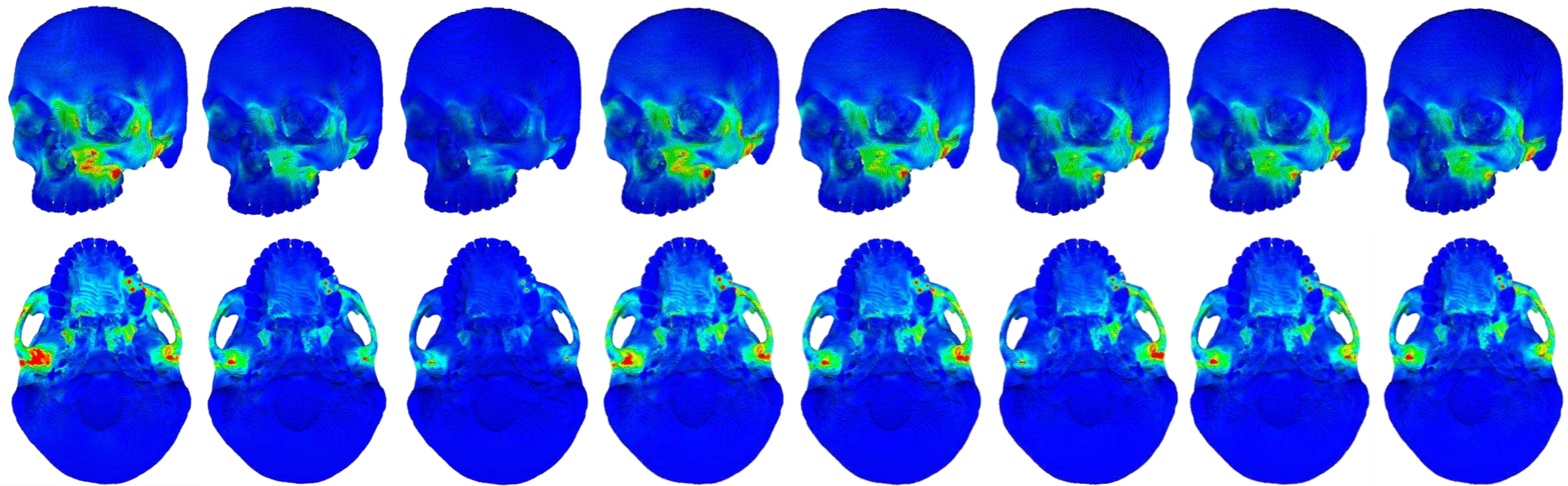
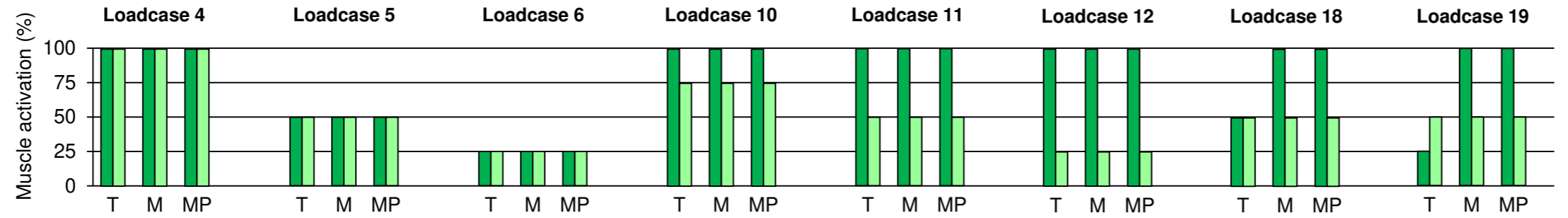
Table 2. Predicted bite and TMJ reaction forces. L=left, R=right, T=temporalis, M&MP=masseter and medial pterygoid muscles. TMJ forces from the working side are marked with an asterisk (\*).

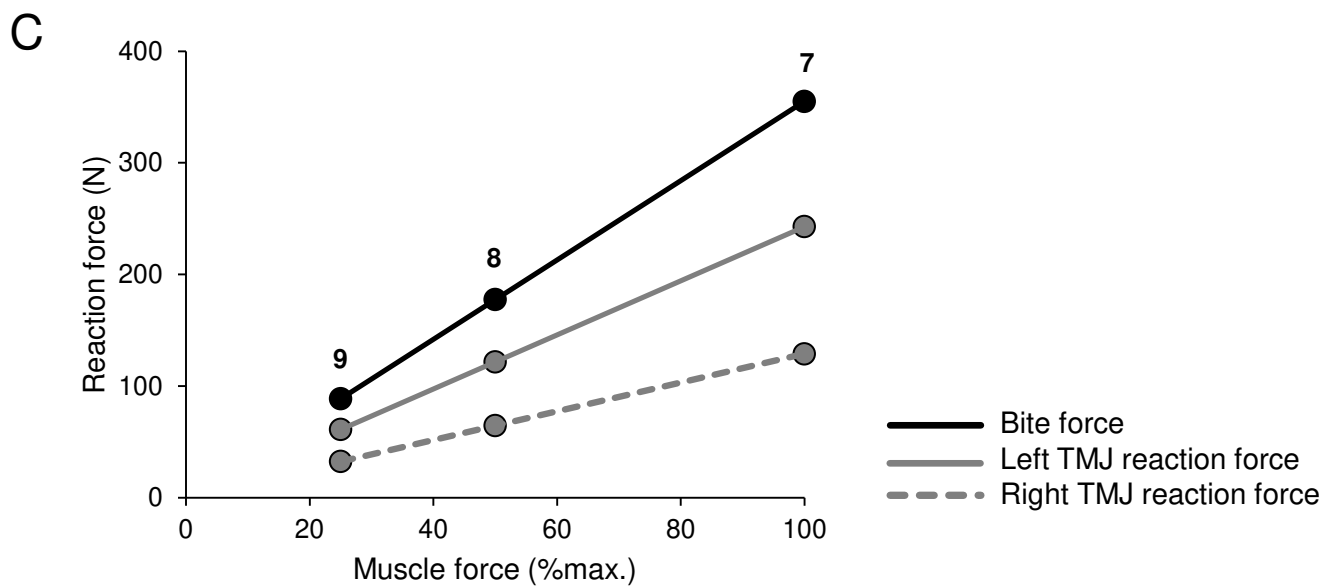
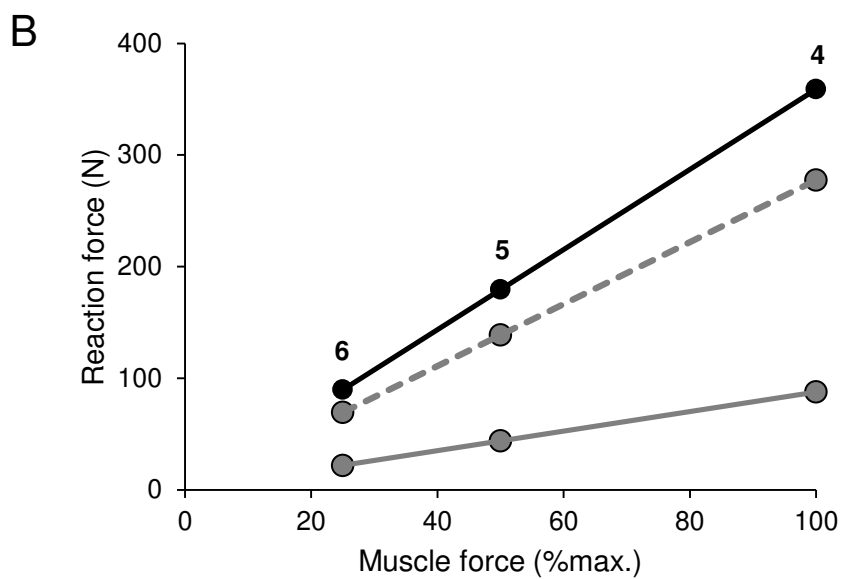
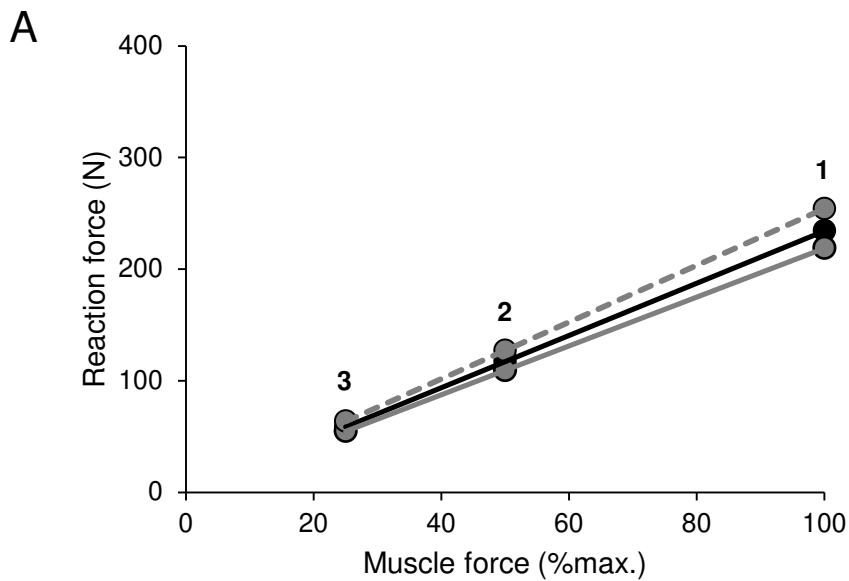
Loadcase	Bite point	Working / balancing side muscle activation	Bite force (N)	TMJ reaction force (N)	
				L-TMJ	R-TMJ
1	L- and R-I <sup>1</sup>	100%/100%	234.29	218.76	254.22
2	L- and R-I <sup>1</sup>	50%/50%	117.15	109.38	127.10
3	L- and R-I <sup>1</sup>	25%/25%	58.60	54.67	63.59
4	L-M <sup>1</sup>	100%/100%	358.91	87.77*	277.53
5	L-M <sup>1</sup>	50%/50%	179.44	43.89*	138.75
6	L-M <sup>1</sup>	25%/25%	89.72	21.95*	69.39
7	R-M <sup>1</sup>	100%/100%	355.09	242.91	128.81*
8	R-M <sup>1</sup>	50%/50%	177.58	121.48	64.42*
9	R-M <sup>1</sup>	25%/25%	88.56	61.01	32.36*
10	L-M <sup>1</sup>	100% / 75%	315.84	110.69*	205.81
11	L-M <sup>1</sup>	100% / 50%	272.73	135.96*	135.74
12	L-M <sup>1</sup>	100% / 25%	229.61	162.43*	72.56
13	R-M <sup>1</sup>	100% / 75%	309.76	174.33	145.76*
14	R-M <sup>1</sup>	100% / 50%	264.27	106.15	166.17*
15	R-M <sup>1</sup>	100% / 25%	220.05	39.99	187.86*
16	L- and R-I <sup>1</sup>	50% (I), 100% (M&MP) / 50% (I), 100% (M&MP)	188.74	176.31	195.99
17	L- and R-I <sup>1</sup>	25% (I), 100% (M&MP) / 25% (I), 100% (M&MP)	165.90	161.85	170.76
18	L-M <sup>1</sup>	50% (I), 100% (M&MP) / 50%	237.59	83.94*	146.09
19	L-M <sup>1</sup>	25% (I), 100% (M&MP) / 50%	219.99	72.50*	151.36
20	R-M <sup>1</sup>	50% (I), 100% (M&MP) / 50%	230.02	120.51	102.51*
21	R-M <sup>1</sup>	25% (I), 100% (M&MP) / 50%	212.79	127.75	77.85*

Table 3. Landmarks for size and shape analysis of global deformation. The landmarks on the zygomatic arch are marked with an asterisk (\*).

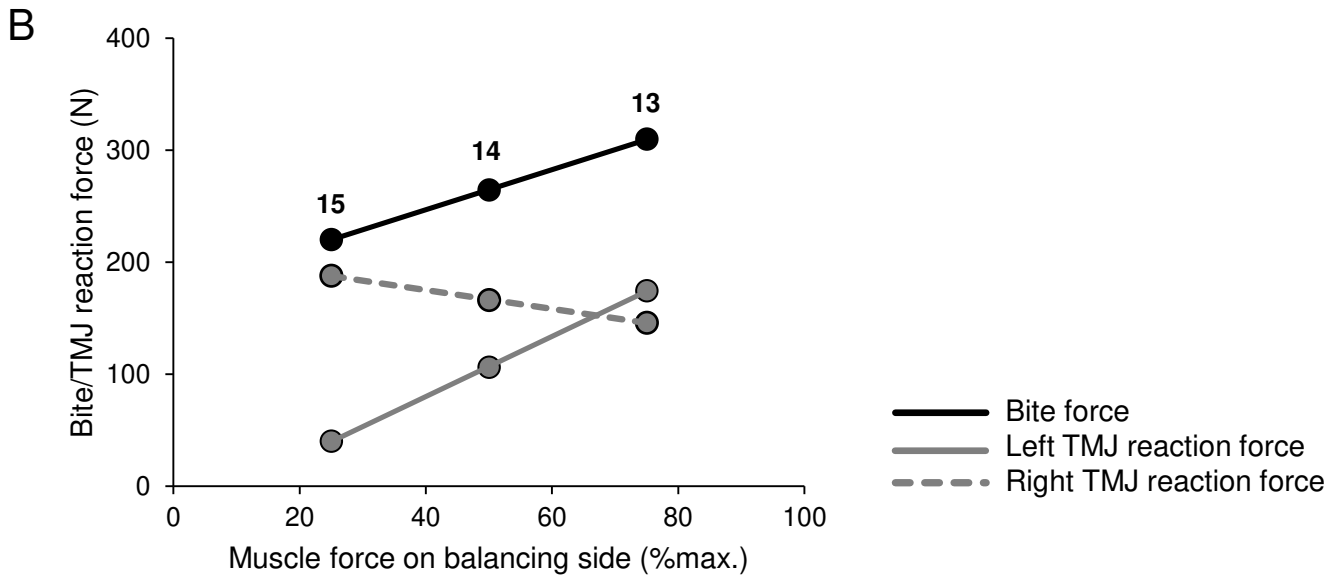
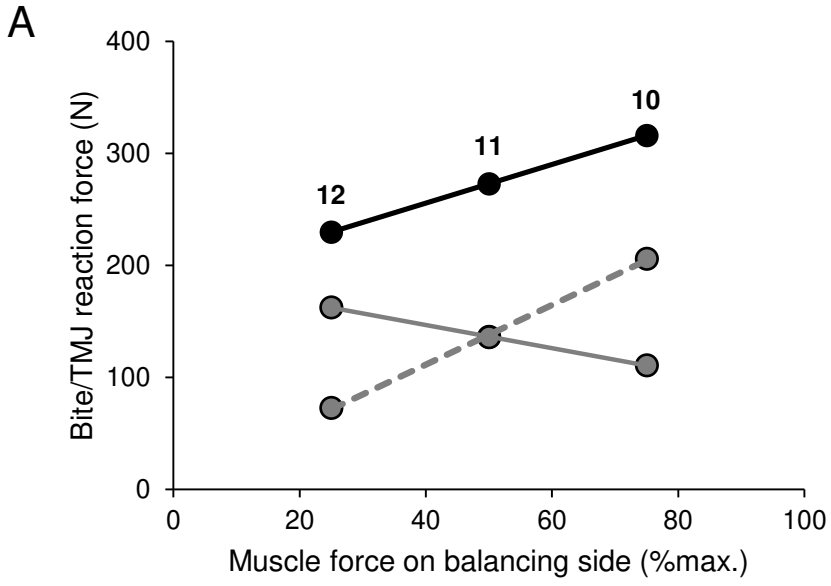
No.	Name	Definition
1	Vertex	Highest point of the cranial vault.
2	Nasion	Intersection between frontonasal and internasal junction.
3	Anterior Nasal Spine	Tip of the anterior nasal spine.
4	Prosthion	Most buccal and occlusal point of the interalveolar septum between central incisors.
5	Occiput	Most posterior point of the cranium.
6&20	Supraorbital Torus	Most anterior point of the supraorbital ridge.
7&21	Infraorbital	Most inferior point of the infraorbital ridge.
8&22	Nasal Notch	Most lateral point of the nasal aperture.
9&23	First Molar	Most buccal and mesial point of the junction of M1 and the alveolar process.
10&24	Last Molar	Most buccal and distal point of the junction between the last molar and the alveolar process.
11&25	Zygo-maxillar	Most inferior point of the zygomatico-maxillary junction.
12&26	Fronto-zygomatic	Most lateral point of the fronto-zygomatic junction.
13&27	Fronto-temporal angle	Point at the intersection between the frontal and temporal processes of the zygomatic bone.
14&28	Zygomatic Arch lateral*	Most lateral point on the zygomatic arch.
15&29	Zygomatic Root posterior	Most posterior-superior point of the intersection between the zygomatic root and the squama of the temporal bone.
16&30	Zygomatic Root anterior	Most anterior point of the intersection between the zygomatic root and the squama of the temporal bone.
17&31	Zygomatic Arch medial*	Most lateral point on the inner face of the zygomatic arch.
18&32	Infratemporal Crest	Most medial point of the infratemporal crest.
19&33	Eurion	Most lateral point of the cranial vault.
34&37	Anterior Temporalis origin	Most anterior point of origin of the temporal muscle in the temporal line.
35&38	Superior Temporalis origin	Most superior point of origin of the temporal muscle in the temporal line.
36&39	Posterior Temporalis origin	Most posterior point of origin of the temporal muscle in the temporal line.
40&43	Anterior Masseteric origin	Most anterior point of origin of the masseter muscle.
41&44	Posterior Masseteric origin*	Most posterior point of origin of the masseter muscle.
42&45	Mid-Masseteric origin*	Midpoint along the origin area of the masseter muscle.
46&49	Superior Pterygoid origin	Most superior point of origin of the medial pterygoid muscle.
47&50	Inferior Pterygoid origin	Most inferior point of origin of the medial pterygoid muscle.
48&51	Mid-Pterygoid origin	Midpoint of the area of origin of the medial pterygoid muscle.

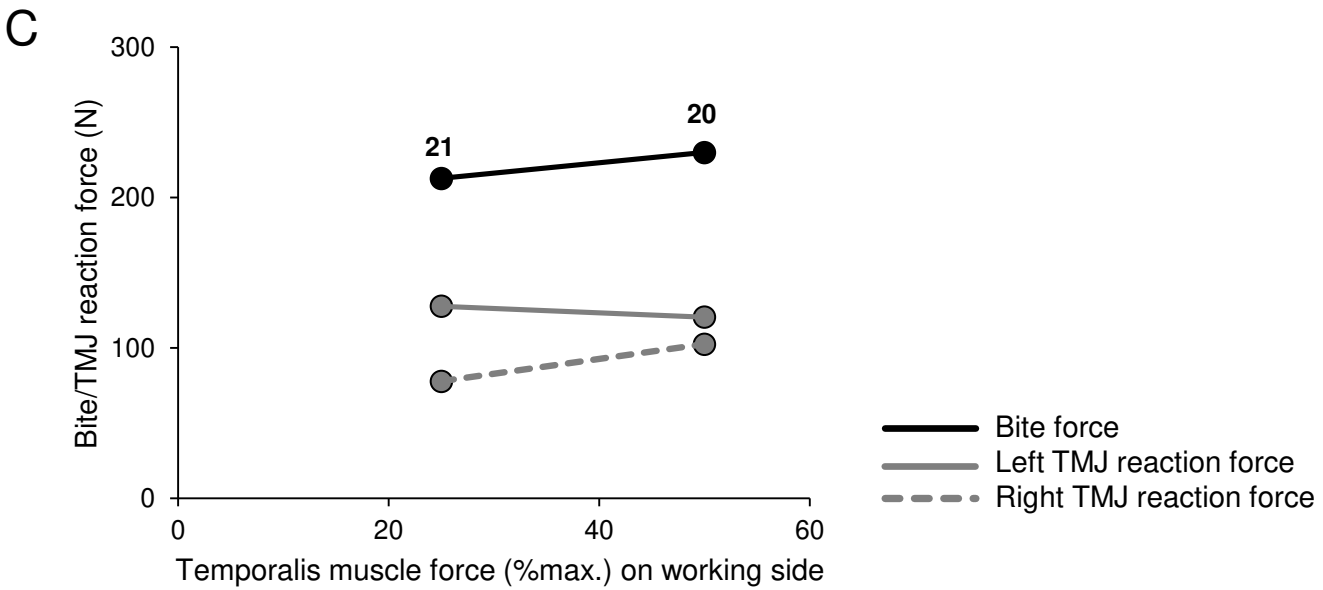
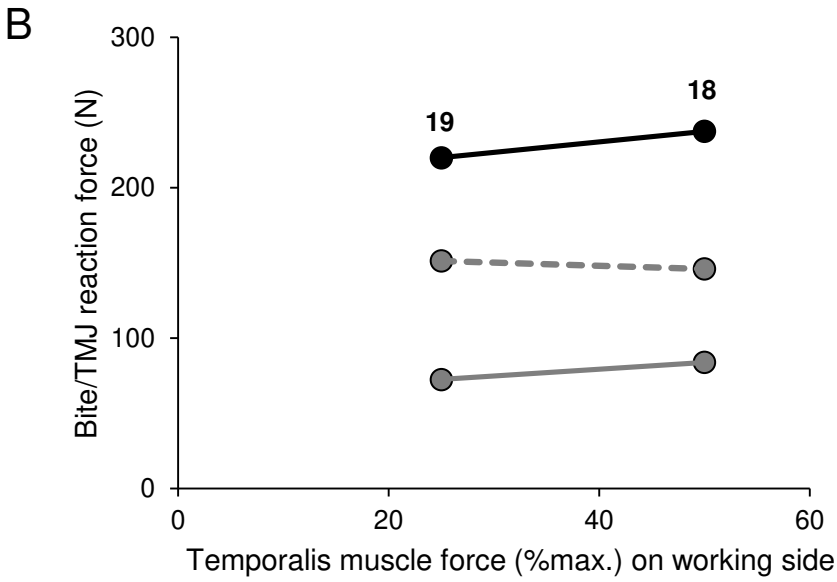
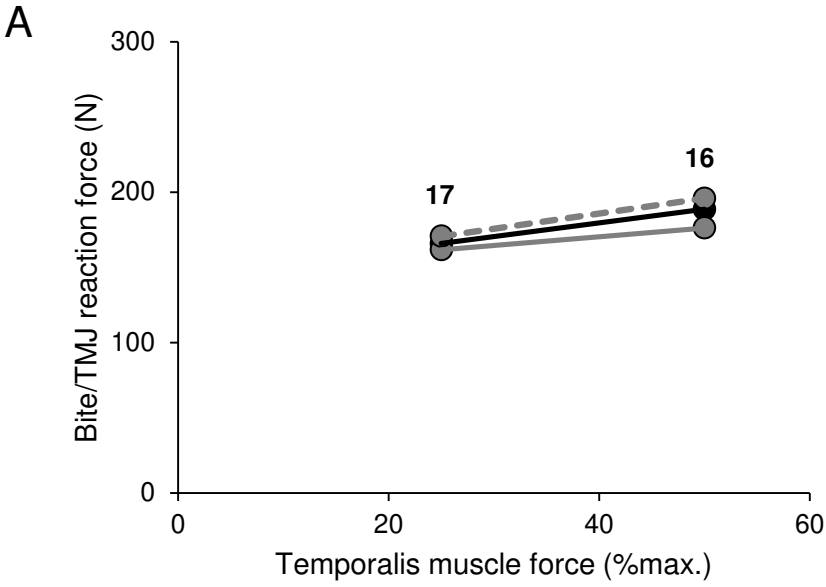


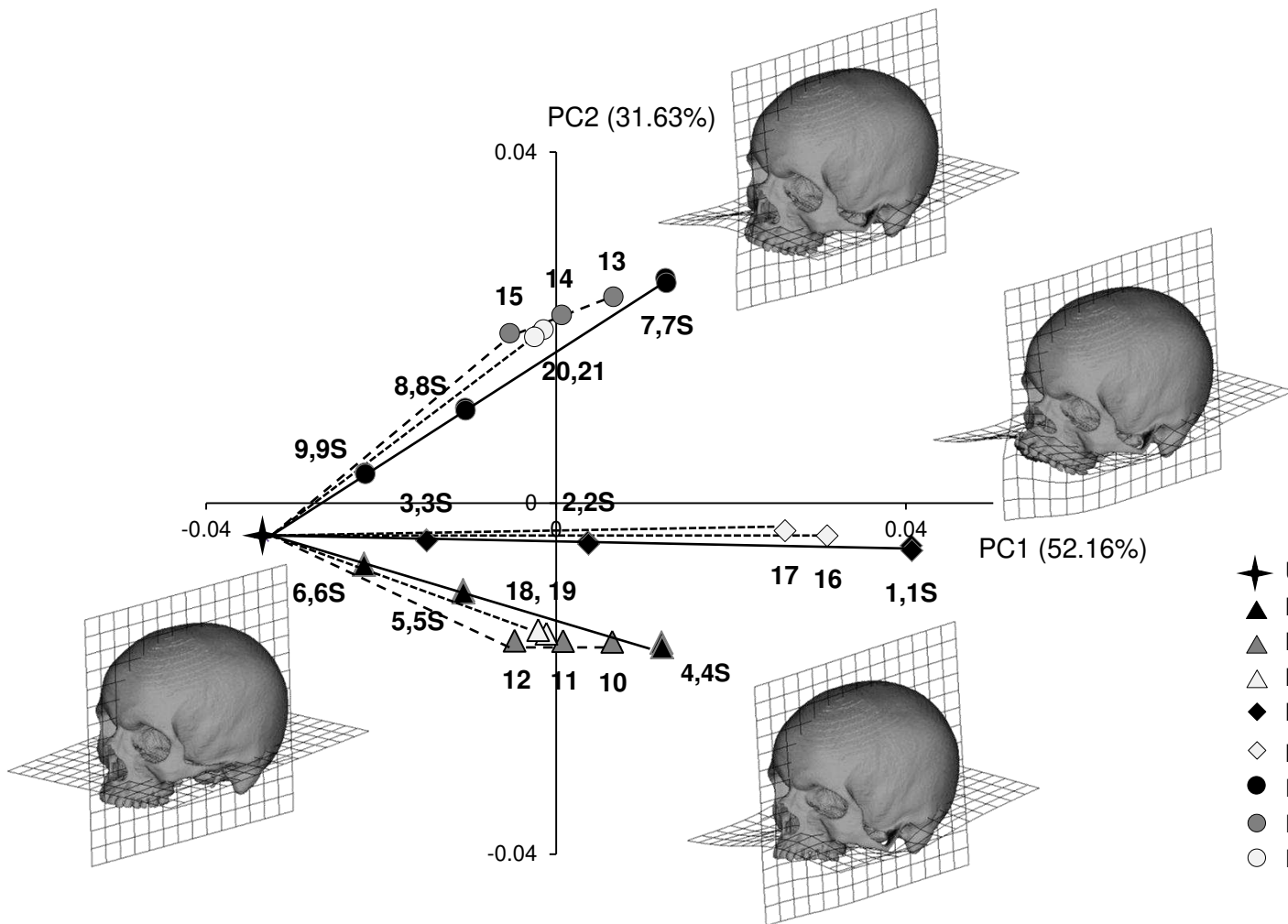




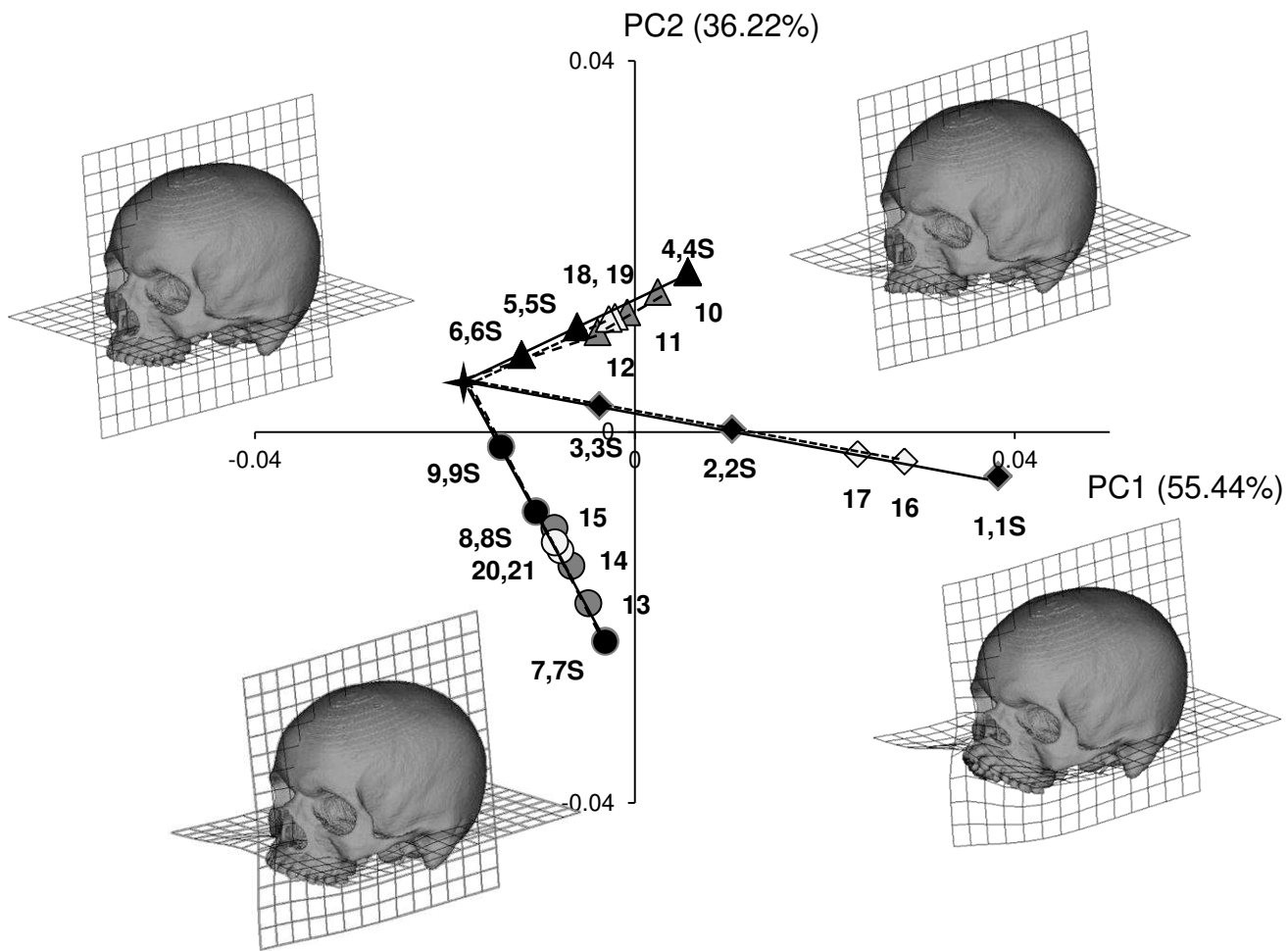








- ✦ Unloaded
- ▲ L-M<sup>1</sup> symmetric, homogeneous
- ▲ L-M<sup>1</sup> asymmetric, homogeneous
- △ L-M<sup>1</sup> asymmetric, heterogeneous
- ◆ L- and R-I<sup>1</sup> symmetric, homogeneous
- ◇ L- and R-I<sup>1</sup> symmetric, heterogeneous
- R-M<sup>1</sup> symmetric, homogeneous
- R-M<sup>1</sup> asymmetric, homogeneous
- R-M<sup>1</sup> asymmetric, heterogeneous



- ✦ Unloaded
- ▲ L-M<sup>1</sup> symmetric, homogeneous
- ▴ L-M<sup>1</sup> asymmetric, homogeneous
- △ L-M<sup>1</sup> asymmetric, heterogeneous
- ◆ L- and R-I<sup>1</sup> symmetric, homogeneous
- ◇ L- and R-I<sup>1</sup> symmetric, heterogeneous
- R-M<sup>1</sup> symmetric, homogeneous
- R-M<sup>1</sup> asymmetric, homogeneous
- R-M<sup>1</sup> asymmetric, heterogeneous